





RESEARCH ARTICLE | AUGUST 25 2022

Air thermochemistry in the converging section of de Laval nozzles on hypersonic wind tunnels

Special Collection: [2022 Chemical Physics](#)Sangdi Gu (顾桑迪)  ; Jiaao Hao (郝佳傲) ; Chih-yung Wen (温志湧) 

AIP Advances 12, 085320 (2022)

<https://doi.org/10.1063/5.0106554>View
OnlineExport
Citation

Articles You May Be Interested In

Analytic energy-level densities of separable harmonic oscillators including approximate hindered rotor corrections

AIP Advances (September 2016)

Investigation on the influence of gas temperature characteristics for engine combustion chamber on plasma jet deflection with MHD control

AIP Advances (August 2022)

Improving the quality of the supersonic flow field of free-jet wind tunnels

AIP Advances (January 2024)



Special Topics Open for Submissions

[Learn More](#)




Air thermochemistry in the converging section of de Laval nozzles on hypersonic wind tunnels

Cite as: AIP Advances 12, 085320 (2022); doi: 10.1063/5.0106554

Submitted: 28 June 2022 • Accepted: 1 August 2022 •

Published Online: 25 August 2022



Sangdi Gu (顾桑迪),^{a)}  Jiaao Hao (郝佳傲),  and Chih-yung Wen (温志湧) 

AFFILIATIONS

The Hong Kong Polytechnic University, Kowloon, Hong Kong

^{a)} Author to whom correspondence should be addressed: sangdi.gu@polyu.edu.hk

ABSTRACT

State-to-state simulations of nonequilibrium flow in nozzles are made for a range of reservoir conditions and geometries. The geometry of the converging section and throat has little influence on the thermochemistry of the flow. Higher reservoir pressure and temperature both drive the thermochemistry toward equilibrium. For reservoir temperatures of 1500, 4000, and 7000 K, the flow property that has the largest departure from equilibrium is the N₂ vibrational temperature, the O mass fraction, and the N mass fraction, respectively. Even at the lowest reservoir pressure, these departures from equilibrium are only 14%, 8%, and 2% for the 1500, 4000, and 7000 K reservoirs, respectively. The differences in these flow properties at the throat between the nonequilibrium and equilibrium simulations are maintained throughout in the nonequilibrium simulations of the diverging section. Applying the simplification of equilibrium flow in the converging section and around the throat yields almost no observable errors in the vibrational population distributions in the diverging section. The simplification is recommended for most practical intents and purposes, and the current work provides important quantitative information to make informed judgments when applying it.

© 2022 Author(s). All article content, except where otherwise noted, is licensed under a Creative Commons Attribution (CC BY) license (<http://creativecommons.org/licenses/by/4.0/>). <https://doi.org/10.1063/5.0106554>

I. INTRODUCTION

The de Laval nozzle is an important component of hypersonic wind tunnels. The numerical simulations of these nozzle flows are often required for flow characterization,¹ test condition design,² and nozzle design purposes.³ Such simulations are usually conducted through the governing flow equations coupled with thermochemical nonequilibrium models, which is essential even under low enthalpy conditions where vibrational excitation is present but no chemical reactions take place.⁴ However, the use of thermochemical nonequilibrium models significantly increases the computational cost, especially when using the high-fidelity state-to-state (StS) nonequilibrium model.⁵ As a result, a simplification for numerical convenience is often made where thermochemical equilibrium, “EQ,” flow is assumed in the converging section and around the throat, allowing the thermochemical nonequilibrium simulation to be performed only for the diverging section (for example, see Refs. 3, 6, and 7).

The aforementioned simplification reduces the computational domain of the nonequilibrium simulation, resulting in computational savings. Apart from this obvious advantage, the simplification

also reduces the computational domain to a purely supersonic flowfield, which allows for a straightforward steady-state analysis where the space-marching⁸ or method of characteristics⁹ techniques can be used to directly solve for the steady state solution. Steady-state analysis is computationally more efficient at solving for the steady state flowfield than time-dependent analysis (time-marching techniques), which usually has to be used if the subsonic portion (converging section) of the flowfield is included in the nonequilibrium simulation due to the strong downstream influence, singularity near the nozzle throat, and unknown mass flow rate.^{8,10} For example, space-marching has been shown to be orders of magnitude faster than time-marching.^{11–13} The use of steady-state analysis is therefore crucial when performing computationally expensive tasks such as nozzle design or StS nozzle simulations. In particular, multi-dimensional StS nozzle simulations, which are computationally too expensive to perform, could be made more practical with the use of steady-state analysis, which would consequently require the use of the aforesaid simplification. A further benefit of the simplification is that it allows for a nozzle flow simulation without needing to know the geometric profile of the converging section because equilibrium flows depend only on the area ratio. Since the profile of the

converging section is often not well documented, especially for nozzles on older wind tunnels, this benefit can be particularly desirable for practical purposes.

However, the validity of this useful simplification is yet to be systematically assessed and characterized for a range of nozzle conditions and geometries relevant to hypersonic wind tunnels. Thus, the current work addresses this important issue because, due to the numerous advantages, it is desirable to use the simplification whenever possible. In this paper, the thermochemical nonequilibrium in the converging section of the de Laval nozzle is examined in detail numerically using the high-fidelity StS model. For comparisons, frozen (calorically perfect gas, “PG”) and equilibrium computations, as well as nonequilibrium computations using the conventional two-temperature (2T) model, are also performed. The entire range of conditions relevant to hypersonic wind tunnels is tested. Different nozzle geometries (converging angle and throat curvature) are investigated as well. The influence on the flow in the diverging section is characterized by the different conditions in the converging section, and the appropriateness of assuming equilibrium flow in the converging section and around the throat for conducting de Laval nozzle simulations is analyzed.

II. METHODOLOGY

An StS model, described in detail in Refs. 5 and 14, is used in the current work. Five species— N_2 , O_2 , N , O , and NO —are considered. There are 61 bound vibrational levels for N_2 , 46 for O_2 , and 48 for NO , all obtained from the STELLAR database.¹⁵ Only the ground electronic state is considered for all species, which is valid since Refs. 16–18 showed that under even higher temperature conditions ($T_0 \approx 9000$ K), ionization and electronic excitation do not play a major role in the thermochemistry of the flow. Along with the vibration–vibration–translation (VVT) and vibration–translation (VT) reactions, the N_2 , O_2 , and NO dissociation/recombination reactions and the two Zel’dovich reactions are modeled. The reactions modeled are summarized in Tables I and II, where “i” and “f” refer to the initial and final vibrational quantum numbers, respectively. The state-specific rates used originate from a combination of Forced Harmonic Oscillator (FHO) theory,¹⁹ quasi-classical trajectory (QCT) calculations,²⁰ and the classic Landau–Teller (LT) model in the StS form.¹⁸ The forward and backward rates are related by detailed balance using the partition functions. Equilibration between translational and rotational modes is assumed.

Due to the computational cost, coupling of a full StS model (unrestricted multi-quantum transitions) with a multi-dimensional flow solver is currently impractical for carrying out a parametric study involving an air mixture ($N_2:0.78$ and $O_2:0.22$ mole fractions), and thus, the inviscid nonequilibrium nozzle flow in this work is modeled based on the quasi-one-dimensional steady Euler equations,^{5,10}

$$\begin{aligned} \frac{d\rho u A}{dx} &= 0, \\ \frac{dp}{dx} + \rho u \frac{du}{dx} &= 0, \\ \frac{dh_0}{dx} &= 0, \\ \frac{dc_i}{dx} - \frac{\dot{w}_i}{\rho u} &= 0, \end{aligned} \quad (1)$$

TABLE I. Inelastic reactions considered in this work, where $M \in \{NO, O, N\}$.

No.	Reaction	Model	References
1	$N_2(i_1) + N_2(i_2) \leftrightarrow N_2(f_1) + N_2(f_2)$	FHO	14
2	$O_2(i_1) + O_2(i_2) \leftrightarrow O_2(f_1) + O_2(f_2)$	FHO	14
3	$O_2(i_1) + N_2(i_2) \leftrightarrow O_2(f_1) + N_2(f_2)$	FHO	14
4	$NO(i) + N_2 \leftrightarrow NO(f) + N_2$	FHO	15
5	$NO(i) + O_2 \leftrightarrow NO(f) + O_2$	FHO	15
6	$NO(i) + M \leftrightarrow NO(f) + M$	LT	18 and 28
7	$N_2(i) + N \leftrightarrow N_2(f) + N$	QCT	29
8	$O_2(i) + O \leftrightarrow O_2(f) + O$	QCT	20
9	$N_2(i) + O \leftrightarrow N_2(f) + O$	LT	18,28
10	$O_2(i) + N \leftrightarrow O_2(f) + N$	LT	18 and 28
11	$N_2(i) + NO \leftrightarrow N_2(f) + NO$	LT	18 and 28
12	$O_2(i) + NO \leftrightarrow O_2(f) + NO$	LT	18 and 28

where ρ is the mass density, u is the flow velocity, A is the nozzle cross-sectional area, p is the pressure, h_0 is the total specific enthalpy, c is the mass fraction, \dot{w} is the mass production rate, and the subscript i is the species index. Because the above-mentioned equations are steady-state ones, time does not appear as a variable, so the equations form an ordinary differential equations (ODE) system. The quasi-one-dimensional model is adequate for revealing basic thermochemical nonequilibrium effects, as demonstrated exemplarily in Refs. 1, 5, 6, and 21–25, by capturing the competition between the flow time and the thermochemical time (analogous to the Damköhler number analysis). The quasi-one-dimensional model assumes that the flow properties are radially uniform at all axial locations along the nozzle. Even if this assumption is violated, which could be for extremely large convergent/divergent angles, the quasi-one-dimensional model will still give a good representative (radially averaged) result and be qualitatively correct because the fundamental flow conservation principles are still obeyed without any

TABLE II. Dissociation/recombination and exchange reactions considered in this work, where $M \in \{NO, O, N\}$.

No.	Reaction	Model	References
1	$N_2(i) + N_2 \leftrightarrow 2N + N_2$	FHO	15
2	$O_2(i) + O_2 \leftrightarrow 2O + O_2$	FHO	15
3	$N_2(i) + O_2 \leftrightarrow 2N + O_2$	FHO	15
4	$O_2(i) + N_2 \leftrightarrow 2O + N_2$	FHO	15
5	$N_2(i) + N \leftrightarrow 3N$	QCT	29
6	$O_2(i) + O \leftrightarrow 3O$	QCT	20
7	$N_2(i) + O \leftrightarrow 2N + O$	Reaction 5	28
8	$O_2(i) + N \leftrightarrow 2O + N$	Reaction 6	28
9	$N_2(i) + NO \leftrightarrow 2N + NO$	Reaction 1	28
10	$O_2(i) + NO \leftrightarrow 2O + NO$	Reaction 4	28
11	$NO(i) + N_2 \leftrightarrow N + O + N_2$	FHO	15
12	$NO(i) + O_2 \leftrightarrow N + O + O_2$	FHO	15
13	$NO(i) + M \leftrightarrow N + O + M$	(Reaction 11) x 20	28
14	$N_2(i) + O \leftrightarrow NO(f) + N$	QCT	30
15	$O_2(i) + N \leftrightarrow NO(f) + O$	QCT	31

compromise.^{26,27} Thus, this model is sufficient for the intents and purposes of the current work.

In the StS model, each vibrational state is considered a pseudo-species. This means that there is no vibrational rate equation and each pseudo-species has a constant vibrational energy corresponding to its vibrational state. In addition, the StS model does not work with vibrational temperatures. Nevertheless, a representative average vibrational temperature for a molecule AB , $T_{V,AB}$, can be obtained by solving the following equation:^{5,14,32}

$$\sum_{v=0}^{v_{\max}(AB)} \frac{\rho_{ABv}}{\rho_{AB}} E_{ABv} = \frac{\sum_{v=0}^{v_{\max}(AB)} E_{ABv} \exp\left(-\frac{E_{ABv}}{k_B T_{V,AB}}\right)}{\sum_{v=0}^{v_{\max}(AB)} \exp\left(-\frac{E_{ABv}}{k_B T_{V,AB}}\right)}, \quad (2)$$

where v is a vibrational level of AB , E is the energy of a vibrational level, and k_B is the Boltzmann constant. The reaction processes considered in this study include $AB(i_1) + CD(i_2) \rightarrow AB(f_1) + CD(f_2)$ VVT transitions (molecule–molecule), $AB(i_1) + M \in \{\text{atoms or molecules}\} \rightarrow AB(f_1) + M$ VT transitions, $AB(i_1) + M \in \{\text{atoms or molecules}\} \rightarrow A + B + M$ vibration-dissociation (VD) reactions, and $AB(i_1) + O/N \leftrightarrow NO(f) + N/O$ exchange reactions. Here, AB and CD represent molecular species while A and B represent atomic species. Considering a molecular species $AB \in \{N_2, O_2\}$ at a vibrational level i_1 , the resulting species production rate can be written generally as^{6,33–35}

$$w_{AB(i_1)} = \mathcal{M}_{AB} \left[\{w_{AB(i_1)}\}_{VVT} + \{w_{AB(i_1)}\}_{VT} + \{w_{AB(i_1)}\}_{VD} + \{w_{AB(i_1)}\}_{EX} \right], \quad (3)$$

where

$$\begin{aligned} \{w_{AB(i_1)}\}_{VVT} &= \sum_{i_2=0}^{i_{2,\max}} \sum_{\substack{f_1=0 \\ f_1 \neq i_1}}^{f_{1,\max}} \sum_{f_2=0}^{f_{2,\max}} k_{VVT}(f_1, f_2 \rightarrow i_1, i_2) \\ &\quad \times X_{f_1} X_{f_2} - k_{VVT}(i_1, i_2 \rightarrow f_1, f_2) X_{i_1} X_{i_2} \end{aligned} \quad (4)$$

for the molecule–molecule interactions and

$$\begin{aligned} \{w_{AB(i_1)}\}_{VT} &= \sum_M \sum_{f_1=0}^{f_{1,\max}} k_{VT}(f_1, M \rightarrow i_1, M) X_{f_1} X_M - k_{VT} \\ &\quad \times (i_1, M \rightarrow f_1, M) X_{i_1} X_M \end{aligned} \quad (5)$$

for the molecule–atom interactions and the molecule–molecule interactions, where VVT reactions are not considered, and

$$\begin{aligned} \{w_{AB(i_1)}\}_{VD} &= \sum_M k_{VD}(A, B, M \rightarrow i_1, M) X_A X_B X_M \\ &\quad - k_{VD}(i_1, M \rightarrow A, B, M) X_{i_1} X_M \end{aligned} \quad (6)$$

for the dissociation/recombination reactions and

$$\begin{aligned} \{w_{AB(i_1)}\}_{EX} &= \sum_{f=0}^{f_{\max}} k_{EX}(NO(f), N/O \rightarrow i_1, O/N) X_{NO(f)} X_{N/O} \\ &\quad - k_{EX}(i_1, O/N \rightarrow NO(f), N/O) X_{i_1} X_{O/N} \end{aligned} \quad (7)$$

for the NO exchange reactions. Here, \mathcal{M} is the molar mass, k is the reaction rate coefficient (calculated from the FHO, QCT, or LT model depending on the reaction, as stated in Tables I and II), and X is the molar concentration. From these, one can easily derive the species production rate for N, O, and $NO(i_1)$.

The solution of Eq. (1) for thermochemical nonequilibrium de Laval nozzle flows is carried out using the methodology in Refs. 36–38, where space marching integration (integration over x) is made using the Crank–Nicolson method, starting from the initial reservoir condition and marching downstream from one point to the next. Based on Ref. 36, the space-marching step size, dx_{s+1} , at a particular step $s + 1$ is governed by the following condition:

$$dx_{s+1} = 10^{-2} \min\left(\frac{q_{s+1}}{|q_{s+1} - q_s|} dx_s\right), \quad (8)$$

where $q \in \{p, T, u, c_i\}$ and $\min()$ is the minimum in the set of values. As discussed by Ref. 36, the step size of these nonequilibrium space-marching solutions is restricted by numerical stability consideration, which is perhaps a bit different from the time-dependent solutions where the distance between spatial points is restricted by discretization error consideration. This is because, as mentioned in Ref. 10, the step size necessary to maintain stability in space-marching is usually much smaller than what is necessary for appropriate spatial discretization, and this will be demonstrated later in Sec. III.

A saddle-point singularity will be encountered during the above-mentioned space marching process. Based on Refs. 10 and 39, Eq. (1) can be combined together with the equation of state and rearranged to give

$$\frac{dT}{dx} = \frac{\frac{A}{\dot{m}} \left(\xi \mathcal{R} T \sum_i \frac{\dot{w}_i}{\mathcal{M}_i} - \sum_i h_i \dot{w}_i \right) - \frac{\xi \mathcal{R} T}{A} \frac{dA}{dx}}{c_{pf} - \xi R}, \quad \xi = \frac{u^2}{u^2 - RT}, \quad (9)$$

where T is the temperature, c_{pf} is the frozen specific heat at constant pressure, h is the specific enthalpy, R is the specific gas constant of the mixture, \mathcal{R} is the universal gas constant, and $\dot{m} = \rho u A$. When u reaches the frozen speed of sound, a_f , which occurs slightly downstream of the throat in a nonfrozen nozzle flow,^{10,25,37} $u = \sqrt{(\gamma RT)}$, where γ is the frozen heat capacity ratio. In turn, $\xi = \gamma/(\gamma - 1)$, and the denominator in Eq. (9) goes to zero, which implies that the numerator must also go to zero for $dT/dx \neq -\infty$. This condition is used to iteratively determine the unknown mass flow rate, \dot{m} , for a given nozzle geometry and reservoir condition.

As shown in Fig. 1, when \dot{m} is too large, dT/dx approaches $-\infty$ as u approaches a_f slightly beyond the throat. In this case, the denominator in Eq. (9) goes to zero before the numerator does. Conversely, when \dot{m} is too small, dT/dx approaches zero before u reaches a_f . In this case, the numerator in Eq. (9) goes to zero before the denominator does. Based on this behavior, a bisection

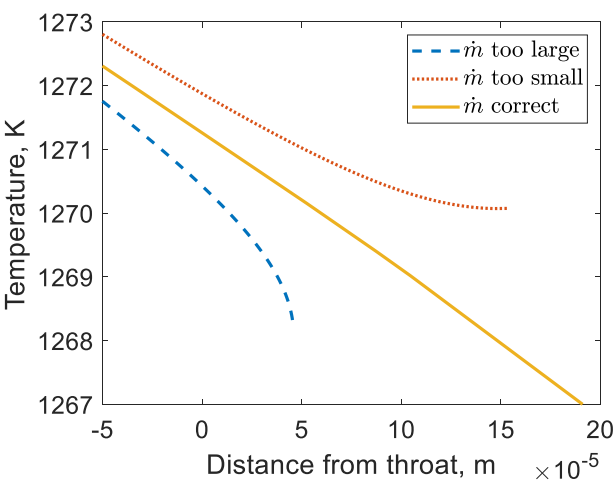


FIG. 1. Computed temperature profile for different values of \dot{m} as u approaches a_f .

method algorithm is set up to iterate for \dot{m} , which takes around one to two hours using the StS model on a single 3.0 GHz Intel i7 CPU. This procedure can be conveniently avoided if equilibrium flow is assumed from the reservoir to a point slightly beyond $u = a_f$, approximately halving the total simulation time. This demonstrates one of the many benefits of this assumption, which are discussed earlier in the Introduction section. As detailed in Ref. 10, equilibrium quasi-one-dimensional nozzle calculations are straightforward, and the methodology is briefly described next.

To compare with nonequilibrium computations, frozen and thermochemical equilibrium results are also obtained. Calculation of the frozen results is trivial, made using the isentropic quasi-one-dimensional nozzle equations with the frozen heat capacity ratio of the reservoir. Computations of the equilibrium, “EQ,” results are made using the conservation of mass and energy equations together with the combined first and second laws of thermodynamics in the form $dh = \frac{dp}{\rho}$ for isentropic flows and the equilibrium state equation, which is given as $h_{eq} = f(\rho, p)$.

III. VALIDATION STUDY

A comparison between steady-state (space-marching) and time-dependent (time-marching) results has often been used for code validation studies.⁴⁰ In Ref. 10, the steady-state analysis of nonequilibrium nozzle flows detailed in Sec. II has been shown to

TABLE III. The reservoir conditions tested in this work, with the reservoir pressure, p_0 , being 1 MPa for all cases.

Case	T_0 , K	N and O mass fractions
1	1500	c_N :0.00, c_O :0.00
2	4000	c_N :0.00, c_O :0.09
3	7000	c_N :0.13, c_O :0.23

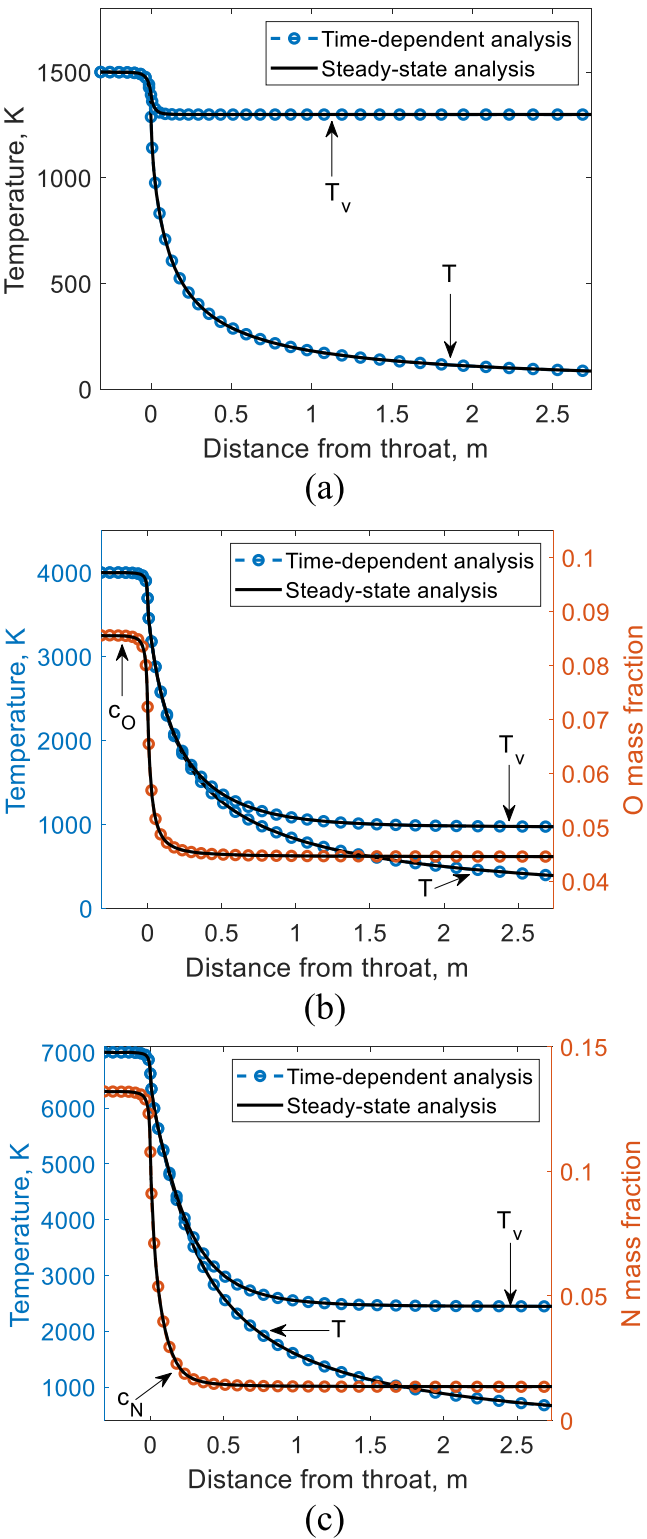


FIG. 2. Temperatures and mass fraction profile through the nominal nozzle (Fig. 3) for test cases (a) 1, (b) 2, and (c) 3 in Table III.

agree well with the time-dependent analysis of Ref. 41, where the unsteady quasi-one-dimensional Euler equations, given as

$$\begin{aligned} \frac{\partial \rho u A}{\partial x} &= -A \frac{\partial \rho}{\partial t} \\ \frac{\partial p}{\partial x} + \rho u \frac{\partial u}{\partial x} &= -\rho \frac{\partial u}{\partial t} \\ p \frac{\partial u}{\partial x} + \rho u \frac{\partial e}{\partial x} + \rho u \frac{\partial \ln(A)}{\partial x} &= -\rho \frac{\partial e}{\partial t} \\ \frac{\partial c_i}{\partial x} - \frac{\dot{w}_i}{\rho u} &= -\frac{1}{u} \frac{\partial c_i}{\partial t}, \end{aligned} \quad (10)$$

are solved, with e being the internal energy per unit mass and t being the time. Further validation is presented here using the 2T model for the conditions (in Table III) tested in the current work.

As shown in Fig. 2, the relevant results between the two types of analysis for all test cases are essentially identical, achieving excellent agreement to within 0.5%. For the time-dependent analysis, the solution is obtained using the methodology outlined in Refs. 10, 26, and 41, where time-marching is carried out via MacCormack's predictor-corrector method and spatial derivatives are evaluated using second-order central difference. A CFL number of 0.5 is used. The spatial dimension is discretized by 375 points with clustering at the throat, where the distance between points is at a minimum of 0.3 mm, achieving grid independence. The same spatial region is integrated in the steady-state analysis using more than 1000 points, which is required in order to maintain numerical stability during the solution. Hypersonic wind tunnel nozzles always operate under under-expanded conditions, so the corresponding boundary conditions used in the time-dependent analysis are those of a subsonic inflow where the velocity is allowed to float and of a supersonic outflow.²⁶ For the steady-state analysis, no boundary condition exists at the outflow, and the flow solution obtained corresponds to that of the underexpanded nozzle. The 2T model used is Park's²⁸ formulation, where molecules are destroyed/created at the average vibrational energy and dissociation/recombination reactions are controlled by $T_c = T^{0.7} T_v^{0.3}$, with T_v being the vibrational temperature. The vibrational energy conservation equation for the time-dependent analysis is expressed as^{42–45}

$$\frac{\partial e_v}{\partial x} - \frac{1}{\rho u} \left(\sum_{i=N_2, O_2, NO} \rho_i \frac{e_{v,i}^{eq} - e_{v,i}}{\tau_v} + e_{v,i} \dot{w}_i \right) = -\frac{1}{u} \frac{\partial e_v}{\partial t}, \quad (11)$$

where e_v and $e_{v,i}$ are the specific vibrational energies of the mixture and species i , respectively, and τ_v is the vibrational relaxation time calculated according to Park's study.²⁸ The vibrational energy conservation equation for the steady-state analysis is the same except that the right-hand side is zero. For the results presented in Fig. 2, the steady-state and time-dependent analyses take a few minutes and around one to two hours, respectively, on a single 3.0 GHz Intel i7 CPU.

Steady-state analysis is often regarded as being more accurate and simpler than time-dependent analysis because the latter needs to deal with iterative convergence, where the residuals [time derivatives in Eq. (10)] need to be eliminated via time-marching, while the former solves directly for the solution, given the time derivatives are equal to zero.⁴⁶ Consequently, along with its superior computational efficiency, the steady-state analysis is preferred over the time-dependent analysis for the current work using the StS model, and all results presented hereafter are calculated using the steady-state analysis.

IV. RESULTS

Simulations are conducted for three different nozzle profiles, shown in Fig. 3. The profiles share the same inlet and throat radii of 70 and 15 mm, respectively, which are representative of an average size hypersonic wind tunnel.^{47–49} The nominal geometry has a 10° half-angle conical converging section connected smoothly (no discontinuity of the gradient) near the throat region with a radius of curvature of two times the throat radius. The throat radius of curvature is generally no smaller than this in order to avoid excessive wall heating.^{50,51} Geometry 2 is the same as the nominal geometry except that the throat radius of curvature is ten times the throat radius, which is generally the upper bound for hypersonic wind tunnel nozzles.⁵² Geometry 3 is the same as the nominal geometry except that the converging section has an 80° half-angle. For all three geometries, the diverging section has a 6° half-angle conical profile, which is typical of the conical nozzles used on hypersonic wind tunnels^{48,49} (large angles are not used to avoid having significantly diverging test flows), connected smoothly to the corresponding throat radius of curvature.

In Ref. 50, it can be seen that the reservoir temperature, T_0 , in hypersonic wind tunnels ranges from around 1500 K to more than 7000 K while the reservoir pressure ranges from around 1–100 MPa. In this paper, the results for the lower bound (1 MPa) of the reservoir pressure are presented first (Secs. IV A and IV B), which correspond

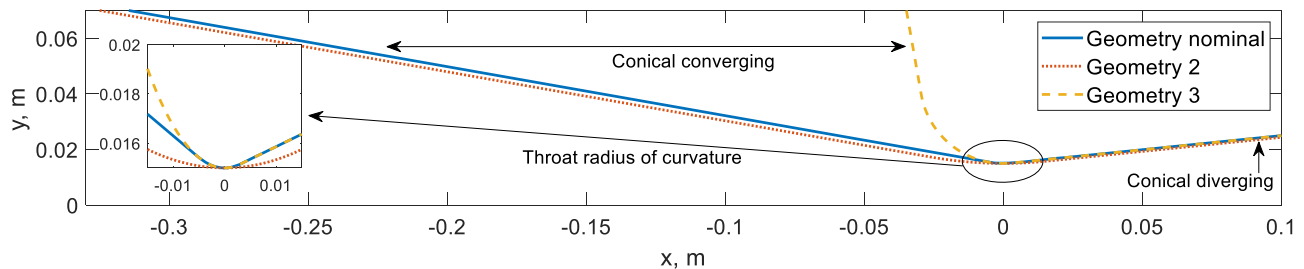


FIG. 3. Nozzle geometries considered in this work.

to the maximum possible departure from equilibrium (lower pressures decrease the molar concentration X resulting in lower values of the mass production rate \dot{w} , as shown in Eq. (3), and drive the solution toward the frozen bound). The influence of higher reservoir pressures is then quantified in Sec. IV C. Reservoir pressures lower than 1 MPa are generally irrelevant in hypersonic wind tunnels due to the need for similarity in parameters matching with the flight while testing with sub-scaled test models.⁵⁰ Three different reservoir temperatures are tested—1500, 4000, and 7000 K. The reservoir is assumed to be in thermochemical equilibrium at the reservoir pressure and temperature. At 1500 K, there is negligible chemical activity as indicated by the lack of molecular dissociation, and thus, only the vibrational nonequilibrium can be important. At 4000 K, there is negligible N_2 dissociation and significant O_2 dissociation. At 7000 K, there is significant N_2 dissociation and complete O_2 dissociation. The test conditions are summarized in Table III.

A. Thermochemistry in the converging section

The translational temperature, T , in a nonequilibrium nozzle flow, when compared to that in a frozen and equilibrium flow, generally provides an overview of the state of the nonequilibrium flow within the equilibrium-frozen spectrum.^{5,10} Figure 4(a) shows an example of the normalized T profiles through the converging section. The StS and 2T nonequilibrium results are bounded by the EQ and frozen (PG) results. The difference between these bounds increases when getting closer toward the throat while the nonequilibrium results depart from the EQ result. Figure 4(b) summarizes the temperature at the throat, T_{throat} , for the three test cases in Table III for the nominal nozzle geometry. For case 1, the nonequilibrium flow is in the middle of the equilibrium and frozen bounds. As T_0 increases, the nonequilibrium flow moves closer toward the equilibrium bound relative to the frozen bound, as shown by the

case 2 and case 3 results. This is due to the faster thermochemical rates at higher temperatures. Nevertheless, the nonequilibrium results differ from the equilibrium results by no more than 3% in all three test cases, and the observation of the nonequilibrium results of case 1 lying in the middle of the frozen and equilibrium bounds is helped by the frozen bound being so close to the equilibrium bound. Finally, comparing the StS and 2T results, the 2T model gives results closer to equilibrium in all three test cases. This finding for the converging section of the de Laval nozzle is consistent with the finding from earlier works on normal shock¹⁴ and purely diverging nozzle⁵ flows where the 2T model was shown to consistently give faster thermochemical relaxation.

For case 1, because no chemical reactions are present as the reservoir temperature is not high enough to cause any significant dissociation of the molecules (Table III), the deviation from equilibrium as shown above in the translational temperature could only be caused by vibrational nonequilibrium. In particular, as shown in Fig. 5(a), it is the vibrational nonequilibrium of N_2 , where the N_2 vibrational temperature (T_{v,N_2}) is around 14% greater than T at the throat, which causes the deviation from equilibrium in the StS result. For cases 2 and 3, vibrational nonequilibrium is found to be negligible, with $T_v/T < 1.001$, and the deviation from equilibrium is mainly caused by chemical nonequilibrium. For case 2, because N_2 is hardly dissociated, it is the finite O recombination rate that causes the deviation from equilibrium, where StS c_O differs by around 8% from equilibrium at the throat, as shown in Fig. 5(b). For case 3, O_2 remains completely dissociated throughout the converging section even in equilibrium, so it is the finite N recombination rate that causes the small deviation from equilibrium, where StS c_N differs by only around 2% from equilibrium at the throat, as shown in Fig. 5(c). Finally, the StS simulations indicate that the vibrational populations of all species are Boltzmann distributed throughout the converging section and around the throat for all cases, as shown in Fig. 6 at the position of the throat.

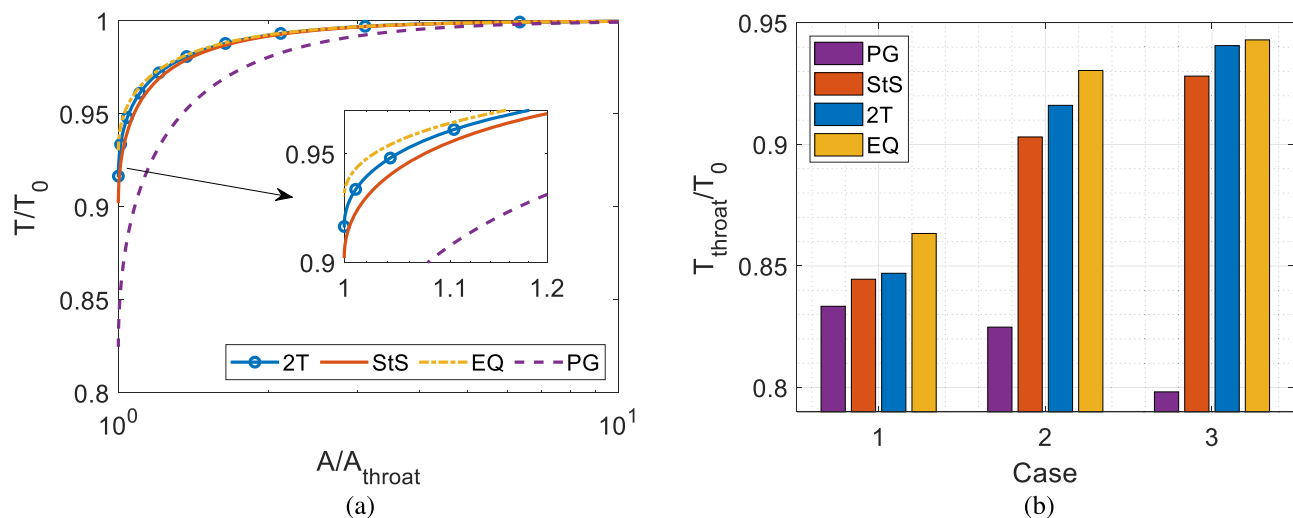


FIG. 4. Normalized temperature profile in the converging section for case 2 is shown in (a). A summary of the results at the throat for all cases is shown in (b). All results shown here are for the nominal geometry.

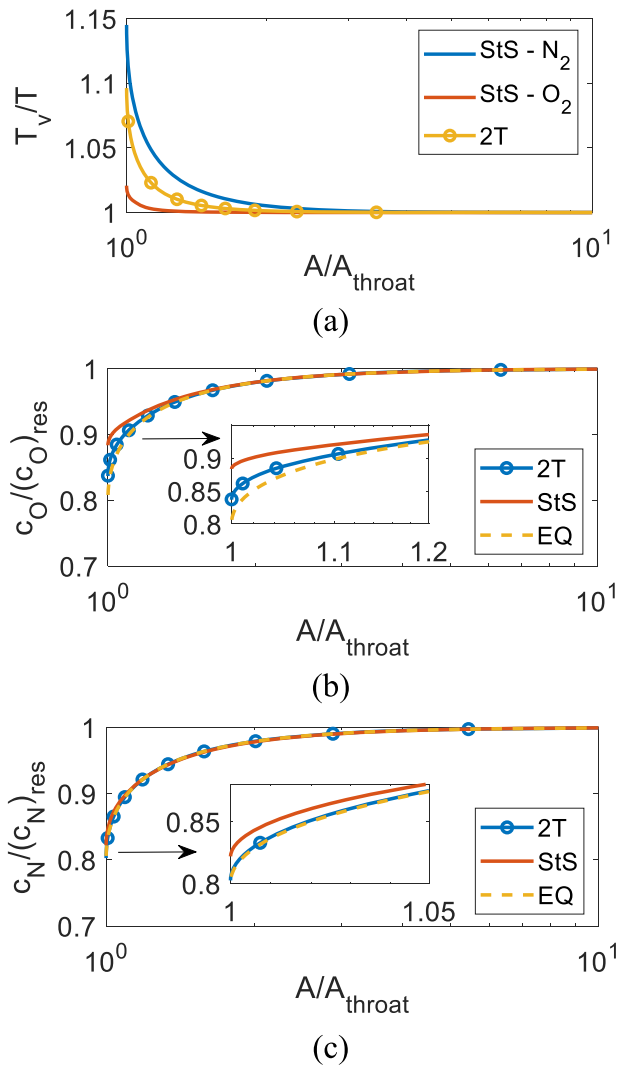


FIG. 5. (a) Vibrational-to-translation temperature ratio for case 1, (b) normalized O mass fraction for case 2, and (c) normalized N mass fraction for case 3. For (b) and (c), the mass fractions are normalized with that at the reservoir. The x-axis is in log scale.

Now, to assess the influence of the geometry of the converging section, the StS thermochemical nonequilibrium results are compared in Fig. 7 between the three very different nozzle geometries shown in Fig. 3. As one would expect in all three conditions, geometry 3 produces the flow with the largest deviation from equilibrium due to the large converging angle, while geometry two produces the flow with the smallest deviation from equilibrium due to the large throat radius of curvature. In general, it can be seen that the geometry of the converging section in hypersonic wind tunnel nozzles is not particularly influential on predicting the flow in the converging section, with such different geometries altering the flow properties by no more than 4% relative to the nominal case in all three conditions. Instead, the choice of the thermochemistry model

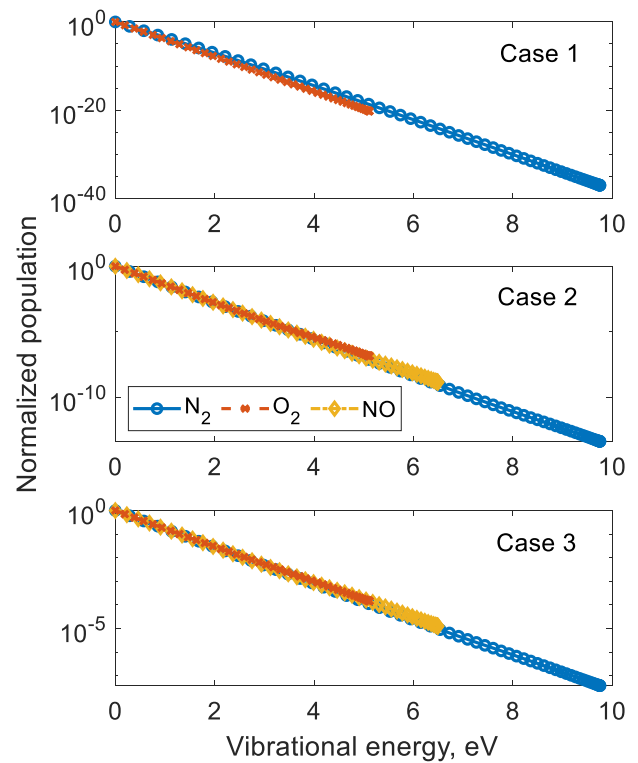


FIG. 6. Vibrational population distributions at the nozzle throat in the nominal nozzle.

(equilibrium, frozen, or nonequilibrium) is more influential on predicting the flow in the converging section.

B. Influence on the diverging flow

Since it is found that some observable departures from equilibrium occur in the converging section in the StS results, it is now of interest to compare the results from the full StS simulation, where the StS model beginning from the reservoir is used, with the results from the simplified StS simulation, where equilibrium flow is assumed from the reservoir until a point slightly beyond $u = a_f$, after which the simulation becomes StS. In Fig. 8, negligible differences of less than 3% are observed in T for all three cases. This means that the differences in T at the throat of less than 3% between the StS and EQ simulations, shown in Fig. 4(b), do not get enlarged in the diverging section. As a result, the differences in the other main flow properties—velocity, pressure, and density—are also negligible. More observable differences are seen in T_{v,N_2} and c_O for cases 1 and 2, respectively. As shown in Figs. 8(a) and 8(b), these flow properties freeze shortly after the throat, and the difference in these flow properties around the throat between the StS nonequilibrium and thermochemical equilibrium simulations, shown in Figs. 5(a) and 5(b), is maintained throughout the diverging section. In case 1, T_{v,N_2} in the diverging section is under-predicted by about 200 K (14%) in the simplified simulation. In case 2, c_O is under-predicted by about 0.005 (8%). As for case 3, because the departure from equilibrium is very small around the throat, as shown in

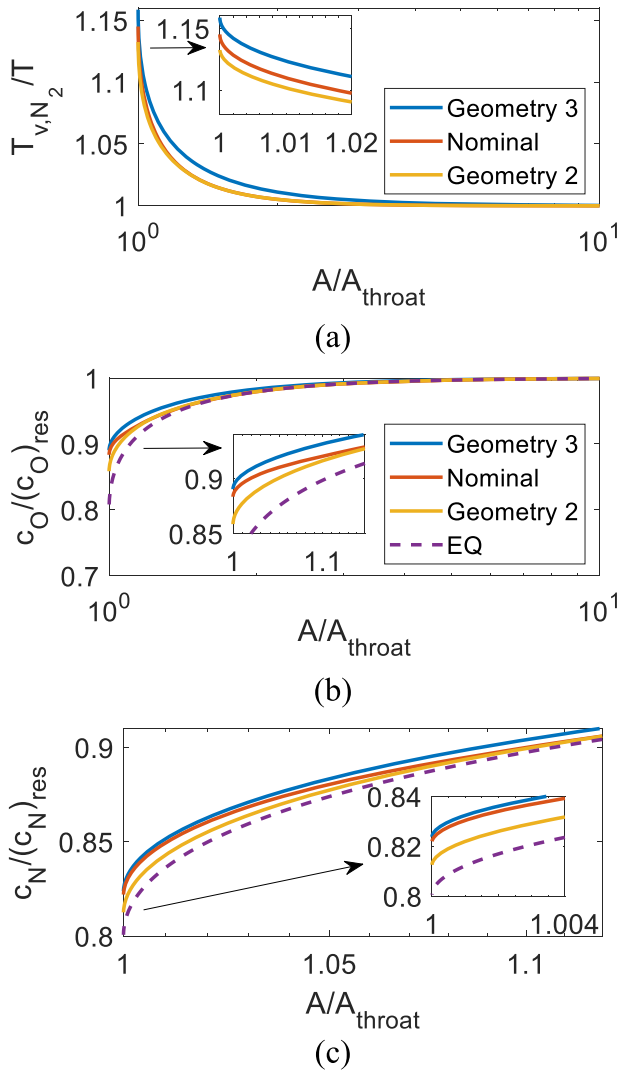


FIG. 7. (a) N_2 vibrational-to-translation temperature ratio for case 1, (b) normalized O mass fraction for case 2, and (c) normalized N mass fraction for case 3 in the different nozzle geometries.

Fig. 5(c), c_N is under-predicted by only about 0.001 (2%) in the simplified StS simulation.

The vibrational population distribution in the diverging section is also assessed, and the result is shown in Fig. 9. In all cases, the population has a non-Boltzmann distribution, which is consistent with prior StS studies on nozzle flows. In cases 2 and 3, the vibrational levels attain a population distribution in the shape of ν , where a near “plateau” region forms around the intermediate levels. Caused by anharmonicity and coupling between the StS thermal and chemical kinetic processes,^{6,32} this trend is commonly observed in nonequilibrium expanding flows as shown numerically^{6,21,22,24,32,53–56} and experimentally.^{57,58} Sometimes, a small peak is formed on the right (higher level) side of the plateau region due to population inversion, as seen in NO and O_2 in case 3 in the current work and in

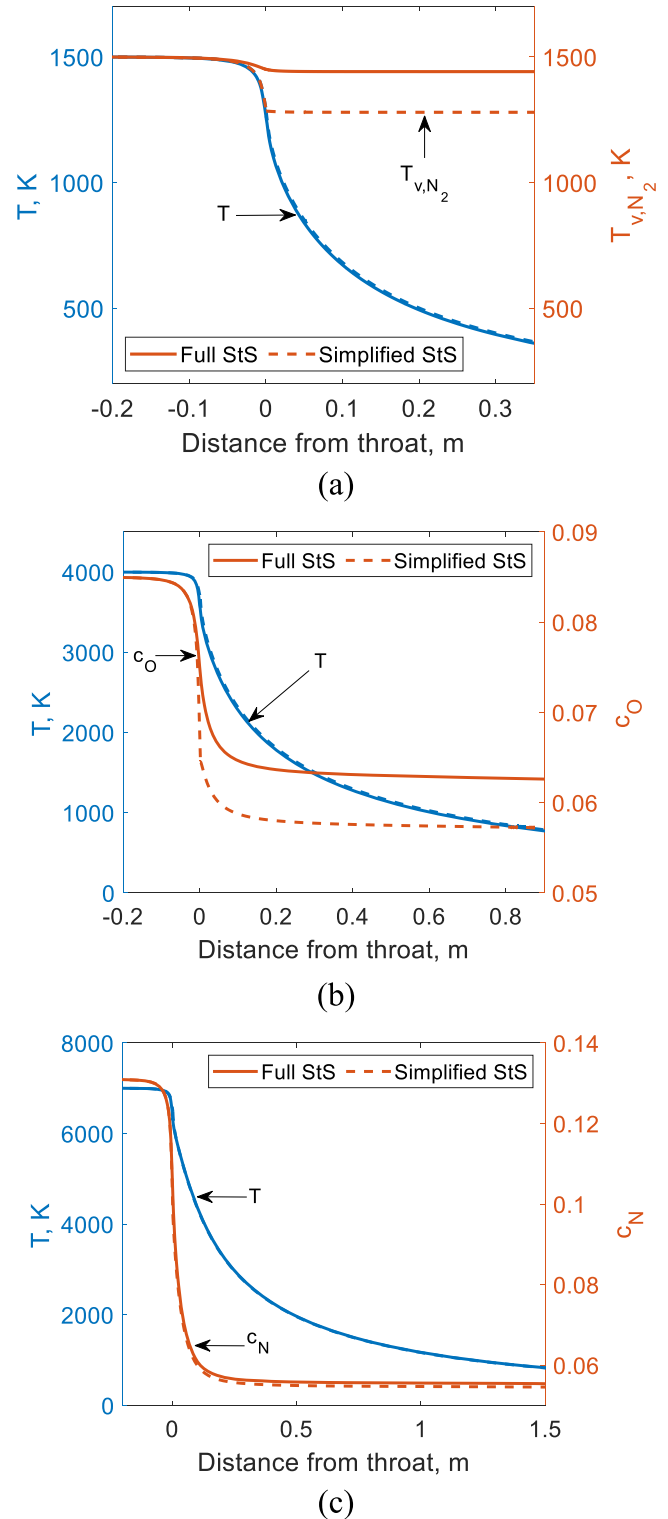


FIG. 8. Translational temperature profiles and vibrational temperature or mass fraction profiles through the nominal nozzle for (a) case 1, (b) case 2, and (c) case 3.

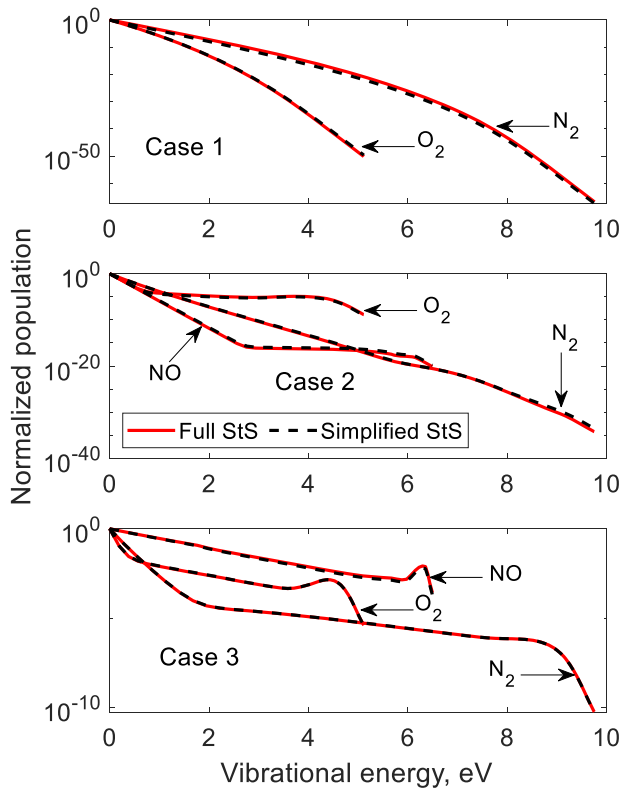
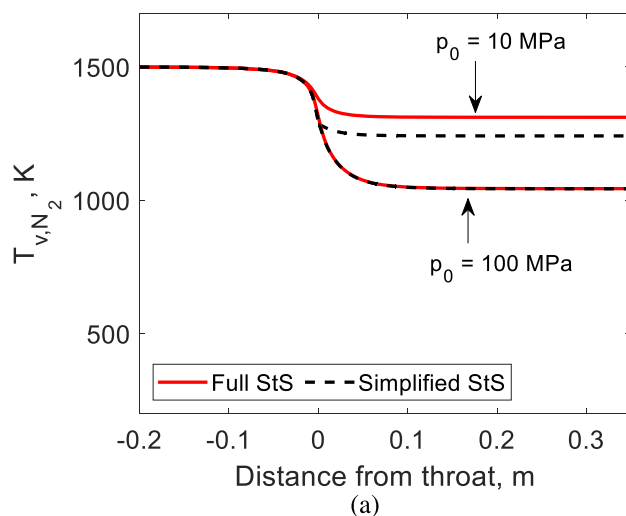


FIG. 9. Vibrational population distributions at 0.3, 0.8, and 1.4 m downstream of the nozzle throat in the nominal nozzle for test cases 1, 2, and 3, respectively.

Refs. 6, 21, 22, 24, 53, and 54. Despite the non-Boltzmann distribution, application of the simplified nozzle simulation yields almost no observable difference in the vibrational population distribution. This is expected because the population distributions are still Boltzmann



distributed near the throat, as shown in Fig. 6, and only becomes non-Boltzmann distributed further downstream in the diverging section.

C. Influence of reservoir pressure

The results presented so far all correspond to a reservoir pressure of 1 MPa, which is the lower bound of the range of reservoir pressures operated in hypersonic wind tunnels, and correspond to the maximum departure from equilibrium. As shown in Fig. 8, while 1 MPa is already enough to have essential equilibrium flow in the converging section and around the throat for case 3, more observable departures from equilibrium are found in cases 1 and 2. Thus, it is now of interest to present some results at higher reservoir pressures at the same reservoir temperatures of these two cases. The results are shown in Fig. 10, comparing the full StS and simplified StS simulations.

As shown in Fig. 10(a) for $T_0 = 1500$ K, compared with the result in Fig. 8(a), increasing the reservoir pressure from 1 to 10 MPa reduces the difference in T_{v,N_2} between the full StS and simplified StS simulations from 200 K (14%) to about 70 K (5%). Further increasing the reservoir pressure to 100 MPa effectively eliminates any difference in T_{v,N_2} between the full StS and simplified StS simulations. For $T_0 = 4000$ K, as shown Fig. 10(b), increasing the reservoir pressure from 1 to 10 MPa effectively eliminates the difference in c_O between the full StS and simplified StS simulations present in the lower pressure. In addition, increasing the reservoir pressure, which helps inhibit molecular dissociation, decreases the atomic mass fraction throughout the flow, as shown in Fig. 10(b), and this reduces the overall influence of thermochemistry on the flow.

V. RECOMMENDATIONS

Overall, applying the simplification of equilibrium flow in the converging section and around the throat leads to only small or negligible errors on the nozzle flow under relevant hypersonic wind tunnel conditions, as shown using the StS model. The simplification

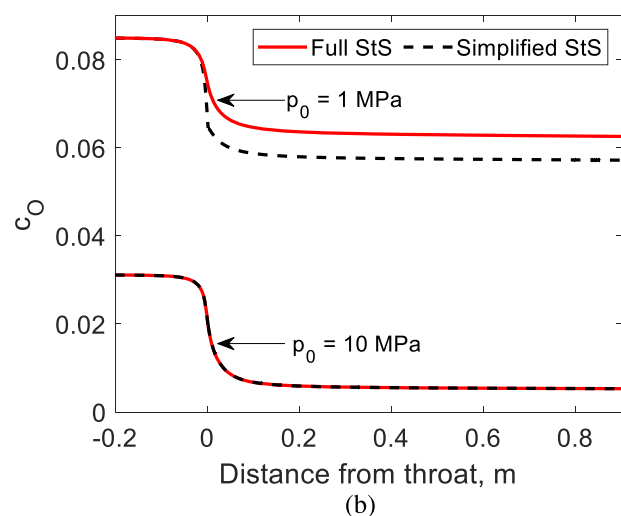


FIG. 10. (a) N_2 vibrational temperature profiles for $T_0 = 1500$ K (case 1) and (b) O mass fraction profiles for $T_0 = 4000$ K (case 2).

works particularly well at higher reservoir pressure and temperature. It would also work better on 2T simulations as the 2T results have closer agreement with equilibrium, as shown in Figs. 4 and 5. The geometry of the converging section and throat has little influence on the thermochemistry of the flow, as shown in Fig. 7, where a significantly larger converging angle or significantly smaller throat radius of curvature is needed to only marginally (<4%) increase the departure from equilibrium. Consequently, application of the simplification can be recommended for most practical intents and purposes, including quasi-one-dimensional parametric studies such as the wind tunnel operating condition mapping in Ref. 2, due to the savings in computation.

Although not directly demonstrated in the current work, which focused on quasi-one-dimensional flows, the full computational benefit of the simplification will be realized when performing two-dimensional nozzle simulations with a steady-state analysis. As shown in Refs. 11–13, for two-dimensional flows, steady-state analysis is orders of magnitude faster than time-dependent analysis, which is usually used for two-dimensional simulations if the subsonic portion (converging section) of the flowfield is included in the simulation. If a simplification is made where a quasi-one-dimensional equilibrium flow is assumed from the reservoir to a point slightly beyond the frozen speed of sound and the flow properties at this said point is used as the inflow for a two-dimensional nonequilibrium nozzle simulation using a steady-state analysis (space-marching or the method of characteristics), orders of magnitude improvements in computational efficiency over nonequilibrium time-dependent analysis can be expected. Such improvements are highly desired for computationally expensive tasks such as nozzle design and StS simulations. Since the results in this paper demonstrate equilibrium flow in the converging section and around the throat, credence is given to the two-dimensional nozzle design methods that implement this simplification, such as Ref. 3, and their usage is recommended. In addition, in light of the result in Fig. 9 showing that applying the simplification yields almost no observable differences in the vibrational population distribution, implementation of the StS model in two-dimensional axisymmetric steady-state nozzle analysis with the simplification is recommended as a future work. Although two-dimensional StS nozzle simulations have been demonstrated in Ref. 59 with a time-dependent analysis, that work used a simplified StS model (single-quantum transitions only) and simulated just a small-scale (≈ 0.1 m length, 65×47 cells) nozzle with only a pure nitrogen mixture. Hence, the steady-state analysis with the simplification, due to its greater computational efficiency, could permit two-dimensional simulations for real-scale wind tunnel nozzles with an air mixture while using higher-fidelity StS models.

Finally, the above-mentioned simplification, where quasi-one-dimensional equilibrium flow analysis is used to determine the supersonic inflow conditions used to start a two-dimensional nozzle simulation, assumes a radially uniform inflow condition. Significant two-dimensional effects on the inviscid flow in the converging section and around the throat could invalidate this assumption, leading to an inaccurate two-dimensional nozzle simulation. This may be seen in nozzles with a large converging angle. In this case, an equilibrium two-dimensional time-dependent analysis should be used instead to obtain the correct nonuniform inflow condition for the nonequilibrium steady-state analysis of the rest of

the nozzle (diverging section), which would still result in significant computational savings when performing nozzle design tasks or StS simulations. Thus, being able to assume equilibrium flow in the converging section and around the throat is beneficial in any case.

VI. CONCLUSIONS

Quasi-one-dimensional StS simulations of inviscid nonequilibrium flow in de Laval nozzles are made. The flow is essentially in equilibrium in the converging section under most conditions relevant to hypersonic wind tunnels, which may be unsurprising given the high number densities and low velocities present. Nevertheless, the current work confirms this result scientifically and systematically. The geometry of the converging section and throat has little influence on the thermochemistry of the flow, needing a significantly larger converging angle or significantly smaller throat radius of curvature to only marginally increase the departure from equilibrium. Higher reservoir pressure and temperature both drive the thermochemistry toward equilibrium. For reservoir temperatures of 1500, 4000, and 7000 K, the flow property that has the largest departure from equilibrium is the N_2 vibrational temperature, the O mass fraction, and the N mass fraction, respectively. Even at the lower bound of the range of reservoir pressures operated in hypersonic wind tunnels (1 MPa), departures from equilibrium of only 14% in the N_2 vibrational temperature, 8% in the O mass fraction, and 2% in the N mass fraction are observed for test cases 1, 2, and 3, respectively. Because these flow properties freeze shortly after the throat, the differences in these flow properties at the throat between the nonequilibrium and equilibrium simulations are maintained throughout in the nonequilibrium simulations of the diverging section. Applying the simplification of equilibrium flow in the converging section and around the throat is recommended for most practical intents and purposes. Because the vibrational population distributions are Boltzmann distributed throughout the converging section and around the throat, applying this simplification yields almost no observable errors in the vibrational population distributions in the diverging section, which become non-Boltzmann distributed downstream. Thus, implementation of the StS model in two-dimensional axisymmetric space-marching and/or the method of characteristics algorithms for two-dimensional StS nozzle simulations is recommended as a future work. The current work provides important quantitative information for engineers and researchers to make informed judgments about applying the simplification.

ACKNOWLEDGMENTS

This work was supported by the first author's start-up fund (Grant No. P0036361) provided by the Hong Kong Polytechnic University.

AUTHOR DECLARATIONS

Conflict of Interest

The authors have no conflicts to disclose.

Author Contributions

Sangdi Gu: Conceptualization (lead); Formal analysis (lead); Investigation (lead); Methodology (lead); Writing – original draft (lead);

Writing – review & editing (equal). **Jiao Hao**: Funding acquisition (equal); Project administration (equal); Resources (equal); Supervision (equal); Writing – review & editing (equal). **Chih-yung Wen**: Funding acquisition (equal); Project administration (equal); Resources (equal); Supervision (equal); Writing – review & editing (equal).

DATA AVAILABILITY

The data that support the findings of this study are available within the article.

REFERENCES

- S. F. Gimelshein and I. J. Wysong, "Nonequilibrium effects in high enthalpy gas flows expanding through nozzles," *Phys. Fluids* **33**, 106104 (2021).
- J. R. Llobet, G. Yamada, and P. Toniato, "Quasi-0D-model mapping of reflected shock tunnel operating conditions," *AIAA J.* **58**, 1668–1680 (2020).
- W. Y. K. Chan, P. A. Jacobs, M. K. Smart, S. Grieve, C. S. Craddock, and L. J. Doherty, "Aerodynamic design of nozzles with uniform outflow for hypervelocity ground-test facilities," *J. Propul. Power* **34**, 1467–1478 (2018).
- P. W. Canupp, G. V. Candler, J. N. Perkins, and W. D. Erickson, "Analysis of hypersonic nozzles including vibrational nonequilibrium and intermolecular force effects," *AIAA J.* **31**, 1243–1249 (1993).
- S. Gu, J. Hao, and C.-Y. Wen, "State-specific study of air in the expansion tunnel nozzle and test section," *AIAA J.* **60**(7), 4024–4038 (2022).
- C. Park, "Thermochemical relaxation in shock tunnels," *J. Thermophys. Heat Transfer* **20**, 689–698 (2006).
- Centre for Hypersonics, The university of queensland, NENZF1d Reference Manual, Retrieved, 26 May 2022, from <https://gdtk.uqcloud.net/docs/nenzf1d/nenzf1d-manual-for-hugo/>.
- C. S. Craddock, "Computational optimization of scramjets and shock tunnel nozzles," Ph.D. thesis, Centre for Hypersonics, Department of Mechanical and Mining Engineering, University of Queensland, Brisbane, Queensland, Australia, 1999.
- W. C. Starshak, C. Butler, and S. J. Laurence, "Method of characteristics design of high-temperature wind tunnel nozzles with vibrational relaxation," in 2018 Aerodynamic Measurement Technology and Ground Testing Conference, Atlanta, Georgia, June 2018.
- J. D. Anderson, "Chapter 17: High-temperature flows," *Modern Compressible Flow: With Historical Perspective*, 4th ed. (McGraw-Hill, New York, 2021).
- K. Srinivas, "An explicit spatial marching algorithm for Navier-Stokes equations," *Comput. Fluids* **21**, 291–299 (1992).
- R. Loehner, "Computational aspects of space-marching," in 36th AIAA Aerospace Sciences Meeting and Exhibit, Reno, NV, January 1998.
- K. Nakahashi and E. Saitoh, "Space-marching method on unstructured grid for supersonic flows with embedded subsonic regions," *AIAA J.* **35**, 1280–1285 (1997).
- S. Gu, J. Hao, and C.-Y. Wen, "On the vibrational state-specific modelling of radiating normal-shocks in air," *AIAA J.* **60**, 3760–3774 (2022).
- M. Lino da Silva, B. Lopez, V. Guerra, and J. Loureiro, "A multiquantum state-to-state model for the fundamental states of air: The stellar database," in *Proceedings of 5th International Workshop on Radiation of High Temperature Gases in Atmospheric Entry* (ESASP, Noordwijk, 2012), Vol. 714, p. 16.
- J. S. Strand and D. B. Goldstein, "Global sensitivity analysis for DSMC simulations of hypersonic shocks," *J. Comput. Phys.* **246**, 184–206 (2013).
- S. F. Gimelshein and I. J. Wysong, "Validation of high-temperature air reaction and relaxation models using emission data," *J. Thermophys. Heat Transfer* **33**, 606–616 (2019).
- W. Su, D. Bruno, and Y. Babou, "State-specific modeling of vibrational relaxation and nitric oxide formation in shock-heated air," *J. Thermophys. Heat Transfer* **32**, 337–352 (2018).
- I. V. Adamovich, S. O. Macheret, J. W. Rich, and C. E. Treanor, "Vibrational energy transfer rates using a forced harmonic oscillator model," *J. Thermophys. Heat Transfer* **12**, 57–65 (1998).
- F. Esposito and M. Capitelli, "The relaxation of vibrationally excited O₂ molecules by atomic oxygen," *Chem. Phys. Lett.* **443**, 222–226 (2007).
- G. Colonna and M. Capitelli, "The influence of atomic and molecular metastable states in high-enthalpy nozzle expansion nitrogen flows," *J. Phys. D: Appl. Phys.* **34**, 1812 (2001).
- G. Colonna and M. Capitelli, "Self-consistent model of chemical, vibrational, electron kinetics in nozzle expansion," *J. Thermophys. Heat Transfer* **15**, 308–316 (2001).
- B. D. Shizgal and F. Lordet, "Vibrational nonequilibrium in a supersonic expansion with reaction: Application to O₂–O," *J. Chem. Phys.* **104**, 3579–3597 (1996).
- G. Colonna, M. Tuttafesta, M. Capitelli, and D. Giordano, "Non-Arrhenius NO formation rate in one-dimensional nozzle airflow," *J. Thermophys. Heat Transfer* **13**, 372–375 (1999).
- J. G. Hall and C. E. Treanor, "Nonequilibrium effects in supersonic-nozzle flows," AGARDograph No 124, 1967.
- J. D. Anderson, "Chapter 7: Numerical solutions of quasi-one-dimensional nozzle flows," *Computational Fluid Dynamics: The Basics with Applications* (McGraw-Hill, New York, 1995).
- J. D. Anderson, "Chapter 5: Quasi-one-dimensional flow," *Modern Compressible Flow: With Historical Perspective*, 4th ed. (McGraw-Hill, New York, 2021).
- C. Park, "Review of chemical-kinetic problems of future NASA missions. I: Earth entries," *J. Thermophys. Heat Transfer* **7**, 385–398 (1993).
- F. Esposito, I. Armenise, and M. Capitelli, "N–N₂ state to state vibrational-relaxation and dissociation rates based on quasiclassical calculations," *Chem. Phys.* **331**, 1–8 (2006).
- D. Bose and G. V. Candler, "Thermal rate constants of the N₂ + O → NO + N reaction using ab initio ³A' and ³A' potential energy surfaces," *J. Chem. Phys.* **104**, 2825–2833 (1996).
- D. Bose and G. V. Candler, "Thermal rate constants of the O₂ + N → NO + O reaction based on the A 2' and A 4' potential-energy surfaces," *J. Chem. Phys.* **107**, 6136–6145 (1997).
- A. Guy, A. Bourdon, and M.-Y. Perrin, "Consistent multi-internal-temperatures models for nonequilibrium nozzle flows," *Chem. Phys.* **420**, 15–24 (2013).
- J. Hao, J. Wang, and C. Lee, "State-specific simulation of oxygen vibrational excitation and dissociation behind a normal shock," *Chem. Phys. Lett.* **681**, 69–74 (2017).
- M. S. Grover, P. Valentini, E. Josyula, and R. S. Chaudhry, "Vibrational state-to-state and multiquantum effects for N₂ + N₂ interactions at high temperatures for aerothermodynamic applications," AIAA Scitech 2020 Forum, AIAA Paper 2020-1227, 2020.
- B. Lopez and M. Lino Da Silva, "Non-Boltzmann analysis of hypersonic air re-entry flows," in 11th AIAA/ASME Joint Thermophysics and Heat Transfer Conference, 2014.
- H. E. Bailey, "Numerical integration of the equations governing the one-dimensional flow of a chemically reactive gas," *Phys. Fluids* **12**, 2292–2300 (1969).
- K. N. C. Bray, "Atomic recombination in a hypersonic wind-tunnel nozzle," *J. Fluid Mech.* **6**, 1–32 (1959).
- R. E. Reichenbach, "Combustion research," Ph.D. thesis, California Institute of Technology, Pasadena, California, 1960.
- G. Emanuel, "A general method for numerical integration through a saddle-point singularity, with application to one-dimensional nonequilibrium nozzle flow," Arnold Engineering Development Center, AEDC-TDR-64-29, 1964.
- R. N. Gupta, J. N. Moss, and A. L. Simmonds, "A comparative study of time-marching and space-marching numerical methods," *AIAA J.* **21**, 145–147 (1983).
- J. D. Anderson, Jr., "Time-dependent solutions of nonequilibrium nozzle flows-A sequel," *AIAA J.* **8**, 2280–2282 (1970).
- J. Olejniczak and G. V. Candler, "Vibrational energy conservation with vibration-dissociation coupling: General theory and numerical studies," *Phys. Fluids* **7**(No. 7), 1764–1774 (1995).

- ⁴³G. V. Candler, "Nonequilibrium hypersonic flows and hypersonic nozzle flow modeling," NATO STO Lecture Series: Flow Characterization and Modeling of Hypersonic Wind Tunnels, STO-AVT-352-VKI, von Karman Institute for Fluid Dynamics, Sint-Genesius-Rode, Belgium, 2018.
- ⁴⁴G. V. Candler, "Rate effects in hypersonic flows," *Annu. Rev. Fluid Mech.* **51**, 379–402 (2019).
- ⁴⁵J. D. Anderson, Jr., "A time-dependent analysis for vibrational and chemical nonequilibrium nozzle flows," *AIAA J.* **8**, 545–550 (1970).
- ⁴⁶A. Savchuk, "Space-marching method on adaptive unstructured grids for supersonic flows," Master of Engineering thesis, Department of Mechanical Engineering, McGill University, Canada, Montreal, Quebec, 2010.
- ⁴⁷A. Gülhan, B. Esser, U. Koch, M. Fischer, E. Magens, and V. Hannemann, "Characterization of high-enthalpy-flow environment for ablation material tests using advanced diagnostics," *AIAA J.* **56**, 1072–1084 (2018).
- ⁴⁸S. Gu, H. Olivier, C.-Y. Wen, J. Hao, and Q. Wang, "Characterization of reflected shock tunnel air conditions using a simple method," *Phys. Fluids* **34**, 056103 (2022).
- ⁴⁹K. Hannemann, J. Martinez Schramm, A. Wagner, and G. Ponchio Camillo, "The high enthalpy shock tunnel Göttingen of the German aerospace center (DLR)," *J. Large-Scale Res. Facilities* **4**, 1–14 (2018).
- ⁵⁰S. Gu and H. Olivier, "Capabilities and limitations of existing hypersonic facilities," *Prog. Aerosp. Sci.* **113**, 100607 (2020).
- ⁵¹H. Hornung, "Performance data of the new free-piston shock tunnel at GALCIT," in 28th Joint Propulsion Conference and Exhibit, Nashville, TN, 1992.
- ⁵²J. Wu and R. Radespiel, "Tandem nozzle supersonic wind tunnel design," *Int. J. Eng. Syst. Modelling Simul.* **47**, 8–18 (2013).
- ⁵³G. Colonna, I. Armenise, D. Bruno, and M. Capitelli, "Reduction of state-to-state kinetics to macroscopic models in hypersonic flows," *J. Thermophys. Heat Transfer* **20**, 477–486 (2006).
- ⁵⁴G. Colonna, L. D. Pietanza, and M. Capitelli, "Recombination-assisted nitrogen dissociation rates under nonequilibrium conditions," *J. Thermophys. Heat Transfer* **22**, 399–406 (2008).
- ⁵⁵A. Sahai, C. O. Johnston, B. Lopez, and M. Panesi, "Flow-radiation coupling in CO₂ hypersonic wakes using reduced-order non-Boltzmann models," *Phys. Rev. Fluids* **4**, 093401 (2019).
- ⁵⁶A. Munafò, M. Panesi, R. Jaffé, G. Colonna, A. Bourdon, and T. Magin, "QCT-based vibrational collisional models applied to nonequilibrium nozzle flows," *Eur. Phys. J. D* **66**, 188 (2012).
- ⁵⁷D. J. Bender, M. Mitchner, and C. H. Kruger, "Measurement of vibrational population distributions in a supersonic expansion of carbon monoxide," *Phys. Fluids* **21**, 1073–1085 (1978).
- ⁵⁸K. P. Horn and P. E. Oettinger, "Vibrational energy transfer in diatomic gas mixtures," *J. Chem. Phys.* **54**, 3040–3046 (1971).
- ⁵⁹M. Tuttafesta, G. Pascazio, and G. Colonna, "Multi-GPU unsteady 2D flow simulation coupled with a state-to-state chemical kinetics," *Comput. Phys. Commun.* **207**, 243–257 (2016).